Multifunctional Ionic Liquids from Rhodium(I) Isocyanide Complexes: Thermochromic, Fluorescence, and Chemochromic Properties Based on Rh-Rh Interaction and Oxidative Addition

Tominaga, Takumi

Mochida, Tomoyuki

(Citation)
Chemistry-A European Journal,24(23):6239-6247

(Issue Date)
2018-04-20

(Resource Type)
journal article

(Version)
Accepted Manuscript

DOI: 10.1002/chem.201800333

Full Paper

Multifunctional Ionic Liquids from Rhodium(I) Isocyanide Complexes: Thermochromic, Fluorescence, and Chemochromic Properties Based on Rh–Rh Interaction and Oxidative Addition

Takumi Tominaga[a] and Tomoyuki Mochida*[a]

Abstract: Square-planar rhodium(I) isocyanide complexes exhibit unique chemical reactivities such as the formation of Rh–Rh bonds and oxidative addition. This paper details the syntheses and properties of multifunctional ionic liquids containing Rh(I) isocyanide complexes [Rh(*n*BuNC)$_4$]X (X = Tf_2N (= $N(SO_2CF_3)_2^-$), Nf_2N (= $N(SO_2C_4F_9)_2^-$), FSA (= $N(SO_2F)_2^-$), $CF_3BF_3^-$). Salts with Tf_2N and Nf_2N were liquids, while those with FSA and CF_3BF_3 were solids at room temperature. The salts exhibited thermochromism in the liquid state, changing from orange at high temperatures to blue-purple at lower temperatures. This is based on the equilibrium between monomer, dimer, and other oligomers associated with Rh–Rh bond formation. The salts also exhibited fluorescence. Exposure of the Tf_2N salt to methyl iodide vapor produced ionic liquid mixtures [Rh(*n*BuNC)$_4$]$_x$[Rh(*n*BuNC)$_4$IMe]$_{(1-x)}$[Tf_2N], concomitant with a color change from purple to red, orange, and yellow, extending the thermochromic color range. The reaction of the Tf_2N salt and iodine produced mononuclear and polynuclear iodine adducts. Thus, these liquids exhibit thermochromism, fluorescence, vapochromism, chemical reactivities, and characteristic properties of ionic liquids.

Keywords: ionic liquids • rhodium • themochromism • thermal properties • oxidative addition

[a] *T. Tominaga, Prof. Dr. T. Mochida*

Department of Chemistry, Graduate School of Science

Kobe University

Rokkodai, Nada, Kobe, Hyogo 657-8501 (Japan)

E-mail: tmochida@platinum.kobe-u.ac.jp

Introduction

Ionic liquids are salts with melting points below 100 °C, exhibiting characteristic features such as negligible vapor pressure, high ionic conductivity, and non-flammability.[1] Ionic liquids are versatile for use in various applications such as electrolytes and reaction solvents. Onium cations and fluorinated anions such as bis(trifluoromethanesulfonyl)amide (Tf_2N) and bis(fluorosulfonyl)amide (FSA) are often used as components of ionic liquids. Recently, ionic liquids with metal-containing anions[2] or cations[3] have been synthesized, and their unique magnetic and fluorescent properties have attracted significant attention. Previously, we have developed various ionic liquids containing cationic metal complexes.[4] Incorporating metal complexes into ionic liquids leads to tunable magnetic properties, catalytic abilities, vapochromism, and thermochromism, which originate from the metal complexes. In this study, multifunctional organometallic ionic liquids containing cationic rhodium isocyanide complexes were designed and synthesized (Figure 1a).

Rhodium(I) isocyanide complexes are cationic square-planar complexes containing d^8 metal ions, which exhibit characteristic chemical reactivities. These complexes can form oligomers, primarily dimers and trimers, by forming Rh–Rh bonds (Figure 2),[5] with each species exhibiting different colors. The UV-vis spectra of their solutions exhibit temperature dependence due to equilibrium between the monomer and oligomers.[6] Several heteroleptic isocyanide complexes bearing *N*-donor bidentate ligands exhibit thermochromism in solutions based on the equilibrium.[7] In addition, these complexes exhibit fluorescence in solution and solid states.[6–8] Rh(I) isocyanide complexes undergo oxidative addition reactions with halogens or alkyl halides to produce octahedral Rh(III) complexes,[9] and this reaction also produces polynuclear complexes. Rh(I) isocyanide complexes have attracted significant attention due to their characteristic reactivities, but their thermal properties have not been characterized.

In this study, we synthesized Rh(I) isocyanide complexes with various anions [Rh(*n*BuNC)$_4$]X ([**1**]X; X = FSA, Tf_2N, CF_3BF_3, Nf_2N (= $N(SO_2C_4F_9)_2^-$); Figure 1a), and characterized their physical properties and chemical reactivities. In addition, the mono- and polynuclear oxidative adducts

[Rh(*n*BuNC)$_4$IMe][Tf$_2$N] ([**1-MeI**][Tf$_2$N]), [Rh(*n*BuNC)$_4$I$_2$][Tf$_2$N] ([**1-I$_2$**][Tf$_2$N]), [{Rh(*n*BuNC)$_4$}$_2$I$_2$][Tf$_2$N]$_2$ ([**2-I$_2$**][Tf$_2$N]$_2$), and [{Rh(*n*BuNC)$_4$}$_3$I$_2$][Tf$_2$N]$_3$ ([**3-I$_2$**][Tf$_2$N]$_3$) were synthesized and characterized (Figure 1b). This study demonstrates that Rh(I)-containing ionic liquids can exhibit thermochromism and fluorescence based on oligomerization via Rh–Rh interactions. Furthermore, the chromic property was tunable by exposure to methyl iodide vapor while maintaining the ionic liquid state. Although many fluorescent ionic liquids have been reported,[10] thermochromic ionic liquids are less common, and most of them are mixtures with additives.[11,12]

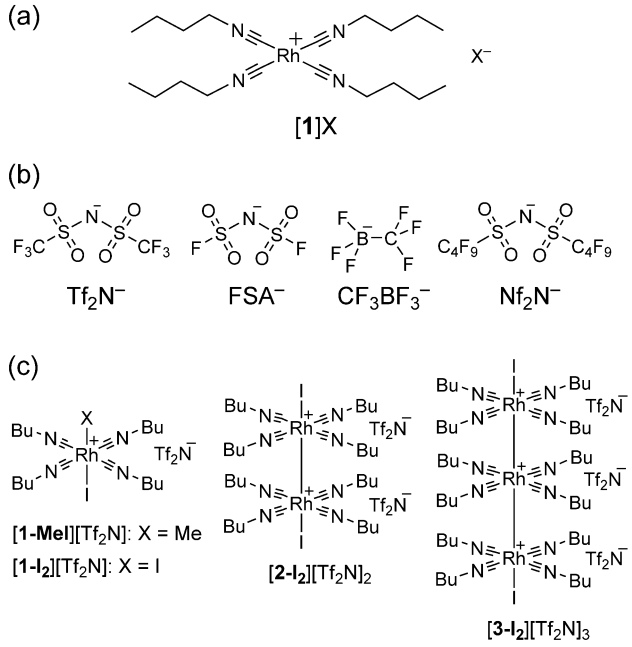

Figure 1. (a) Ionic liquids containing rhodium(I) isocyanide complexes synthesized in this study ([**1**]X), (b) the counter anions used (Tf$_2$N, Nf$_2$N, FSA, and CF$_3$BF$_3$), and (c) oxidative adducts synthesized from [**1**][Tf$_2$N] ([**1**-MeI][Tf$_2$N], [**1-I$_2$**][Tf$_2$N], [**2-I$_2$**][Tf$_2$N], and [**3-I$_2$**][Tf$_2$N]$_3$).

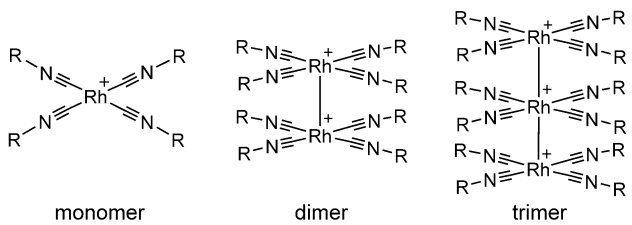

Figure 2. Structure of the monomer, dimer, and trimer of Rh(I) isocyanide complexes.

Results and discussion

Synthesis and thermal properties of [1]X and [1-MeI][Tf_2N]

[**1**]X (X = Tf_2N, Nf_2N, FSA, CF_3BF_3) was synthesized via the [**1**]Cl precursor, which was prepared by the reaction of $[Rh(C_8H_{12})Cl]_2$ and BuNC, followed by anion exchange with alkali metal salts of the corresponding anions (60–80% yield). The thermodynamic data for the synthesized complexes obtained by DSC measurements are shown in Table 1 and their DSC traces are shown in Figure S1 (supporting information).

[**1**][Tf_2N] and [**1**][Nf_2N] (T_m = 10.5 °C) were purple liquids, whereas [**1**][FSA] (T_m = 77.4 °C) and [**1**][CF_3BF_3] (T_m = 84.0 °C) were purple crystals at room temperature. Therefore, the smaller anions resulted in higher melting points. [**1**][Tf_2N] did not solidify and exhibited only a glass transition (T_g = –85 °C). [**1**][Nf_2N] exhibited also a glass transition at T_g = –69 °C on rapid cooling, and the ratio of the glass transition temperature to melting point for this salt (T_g/T_m = 0.72) was consistent with the empirical rule for molecular liquids (T_g/T_m = 2/3).[13] In addition, [**1**][FSA] and [**1**][CF_3BF_3] exhibited a phase transition in the solid state at –123.4 °C (ΔS = 24.6 J K^{-1} mol^{-1}) and –135.0 °C (ΔS = 14.8 J K^{-1} mol^{-1}), respectively.

The reaction of [**1**][Tf_2N] and methyl iodide in dichloromethane produced an oxidative adduct [**1-MeI**][Tf_2N] (T_m = 32.2 °C), which was a pale-yellow powder. This salt maintained a liquid state at room temperature after melting, undergoing crystallization at approximately –10 °C or a glass transition (T_g = –66 °C) depending on the cooling rate. The ratio of the glass transition temperature to melting point (T_g/T_m = 0.68) was consistent with the empirical rule.[13] The reaction occurred readily, hence the exposure of [**1**][Tf_2N] to a vapor of methyl iodide easily produced ionic liquid mixtures [**1**]$_x$[**1-MeI**]$_{(1-x)}$[Tf_2N] (Figure 3), which changed from purple (x = 1) to red (x = 0.66), orange (x = 0.26), and yellow (x = 0.03). This vapochromic behavior was irreversible, and heating the product did not recover the starting material (see below). However, we found that UV irradiation of [**1-MeI**][Tf_2N] in the solid or liquid state causes partial elimination of methyl iodide accompanying a prominent color change from pale yellow to red (Figure S2, supporting information).

Table 1. Thermodynamic data of the salts synthesized in this study.

	T_m (°C)	T_g (°C)	ΔH (kJ mol^{-1})	ΔS_m (J K^{-1} mol^{-1})	T_{dec} (°C)[a]
[**1**][Tf_2N]		–85			265
[**1**][Nf_2N]	10.5	–69			276
[**1**][FSA]	77.4		24.2	68.7	255
[**1**][CF_3BF_3]	84.0		19.9	55.6	258
[**1-MeI**][Tf_2N]	32.2	–118	30.6	99.8	114[b]
[**1-I$_2$**][Tf_2N]	119.1		41.6	105.7	247
[**2-I$_2$**][Tf_2N]$_2$	47.4	–54	36.1	112.2	
[**3-I$_2$**][Tf_2N]$_3$	46.4	–52	66.8	207.4	

[a] Decomposition temperature (–3 wt%) determined by TG measurement.
[b] Temperature at which a chemical reaction occurred.

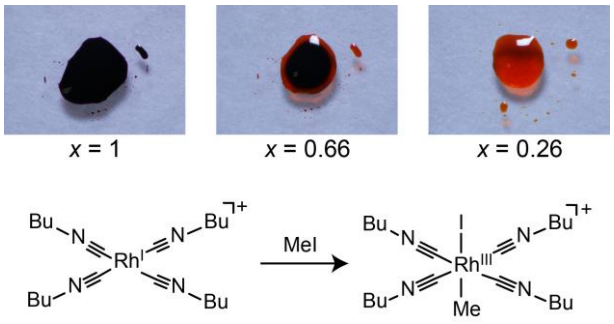

Figure 3. Color change of [**1**][Tf_2N] upon addition of methyl iodide. Addition ratio (x) ([**1**]$_x$[**1-MeI**]$_{(1-x)}$[Tf_2N]) is indicated beneath each of the photographs. Reaction scheme is also shown below the photos.

Thermochromism

[**1**]X exhibited thermochromism in the liquid state and photographs of [**1**][Tf_2N] are shown in Figure 4 and Figure S3 (supporting information). The color of the ionic liquid was orange at 100 °C, purple at 0 °C, and blue-purple at –100 °C, and [**1**][Nf_2N] exhibited similar color changes. [**1**][FSA] was purple-pink in the solid state, and it exhibited thermochromism in the liquid state (100–40 °C), changing from orange at 100 °C to pink at 40 °C.

The thermochromism of [**1**][Tf_2N] could be controlled by reaction with methyl iodide vapor. Photographs of [**1**]$_x$[**1-MeI**]$_{(1-x)}$[Tf_2N] (x = 0.35, 0.03) are shown in Figure 5 and Figure S4

(supporting information). The x = 0.35 sample was pale pink at 60 °C and red at –100 °C (Figure 5a), whereas the x = 0.03 sample turned from pale yellow at 60 °C to orange at –100 °C (Figure 5b). The change of the thermochromic color range can be ascribed to the dilution of the purple thermochromic ionic liquid in a yellow non-thermochromic ionic liquid and a decrease of the oligomer ratio.

Plots of the thermochromic color ranges of [**1**][Tf_2N] and [**1**]$_x$[**1-MeI**]$_{(1-x)}$[Tf_2N] in color space, derived from their UV-vis spectra recorded between −100 and 60 °C (vide infra), are shown in Figure 6 and Figure S5 (supporting information). A dichloromethane solution of [**1**][Tf_2N] exhibited thermochromism between yellow and red, though the ionic liquids have a wider color range extending from blue-purple to pale yellow. This was achieved through the highly concentrated state of the cations in the neat ionic liquids.

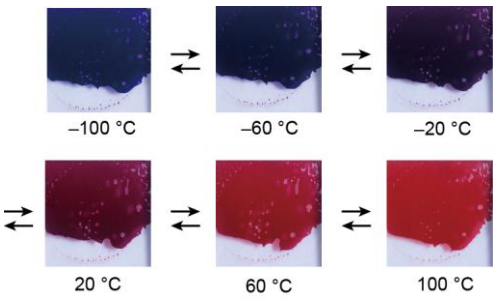

Figure 4. Photographs of the liquid sandwiched between quartz plates demonstrating the thermochromism of [**1**][Tf_2N].

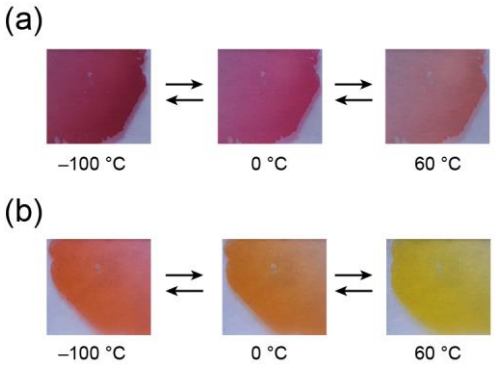

Figure 5. Photographs of the liquid sandwiched between quartz plates demonstrating the thermochromism of [**1**]$_x$[**1-MeI**]$_{(1-x)}$[Tf_2N] (x = 0.35 (a), 0.03 (b)).

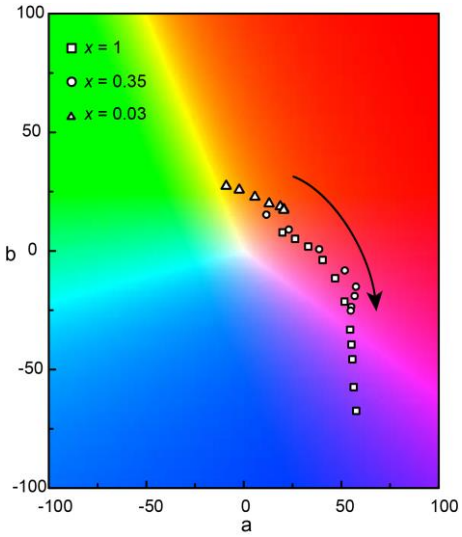

Figure 6. Thermochromic color range of [**1**]$_x$[**1-MeI**]$_{(1-x)}$[Tf_2N] (x = 1 (□), 0.35 (○), 0.03 (△)) between −100 and 60 °C displayed in Lab color space. The arrow indicates direction of color change upon cooling.

UV-vis spectra

The temperature dependence of the UV-vis spectra of [**1**][X] (X = Tf_2N, Nf_2N, FSA) and [**1**]$_x$[**1-MeI**]$_{(1-x)}$[Tf_2N] was measured. In all samples, the ratio of oligomers, including dimers, increased at lower temperatures in the liquid state, which caused the thermochromism.

The UV-vis spectra of [**1**]X at room temperature are shown in Figure 7a. Rh(I) isocyanide complexes generally exhibit absorption bands of monomers, dimers, and trimers at approximately 380, 520, and 650 nm, respectively, which are ascribed to the $d_z^2 \rightarrow p_z$ (Rh^I) transition.[5] The peaks corresponding to the monomer and dimer were observed in the spectra of [**1**][Tf_2N] and [**1**][Nf_2N], indicating that both species exist in the liquids. However, only the absorption of the dimer (550 nm) was observed in the spectra of [**1**][FSA] and [**1**][CF_3BF_3], indicating that these solids contain only dimers. The dimer absorption in the solids exhibited a redshift by approximately 20 nm compared to the liquid state, which can be attributed to the shorter Rh–Rh distances in the solids.[7] The oxidative adduct [**1-MeI**][Tf_2N] exhibited an absorption peak at a shorter wavelength around 317 nm (Figure S6, supporting information).

The temperature dependence of the UV-vis spectra of [**1**][Tf_2N] is shown in Figure 8a. The absorbance intensities of the monomer, dimer, and trimer peaks are shown as function of temperature in the inset of the figure. Upon cooling, the oligomer ratio increased at low temperatures. The monomer peak (~390 nm) gradually decreased, concomitant with the increase in the intensity of the dimer (~520 nm) and trimer (~650 nm) peaks. In addition, a small peak appeared at approximately 800 nm at low temperatures, which was ascribed to oligomers larger than a tetramer.[7] The dimer and trimer peaks exhibited red shifting upon cooling, which is ascribed to shortening of the Rh–Rh bond at lower temperatures.[7] [**1**][Nf_2N] and [**1**][FSA] exhibited a similar temperature dependence in the liquid state (Figure S7, supporting information). These samples crystallized at approximately –10 and 30 °C, respectively, and only the dimer band was observed in the solid state.

The ability to form oligomers in the liquid state differed between [**1**][Tf_2N], [**1**][Nf_2N], and [**1**][FSA]. Comparison of their spectra at the same temperature indicates that the ratio of oligomer to monomer follows the order [**1**][Tf_2N] < [**1**][Nf_2N] < [**1**][FSA] (Figure S8, supporting information). This is in agreement with the melting point and glass transition temperature trends (T_g ([**1**][Tf_2N]) < T_g or T_m ([**1**][Nf_2N]) < T_m ([**1**][FSA])). It seems reasonable that the salts forming oligomers more effectively have higher melting points and glass transition temperatures.

The temperature dependence of the UV-vis spectra of [**1**]$_x$[**1-MeI**]$_{(1-x)}$[Tf_2N] (x = 0.51, 0.11) are shown in Figure 8b, c. The absorption intensity of the dimer (~520 nm) and trimer (~650 nm) peaks increased upon cooling, similar to those of [**1**][Tf_2N]. Increases in the amount of methyl iodide adducts decreased the oligomer ratio. In contrast to the spectra of [**1**][Tf_2N], the absorption maximum of the dimers exhibited a slight blue-shift upon cooling. This tendency may suggest that the bond in the dimer weakens at lower temperatures in the presence of [**1-MeI**][Tf_2N], though the mechanism is unclear.

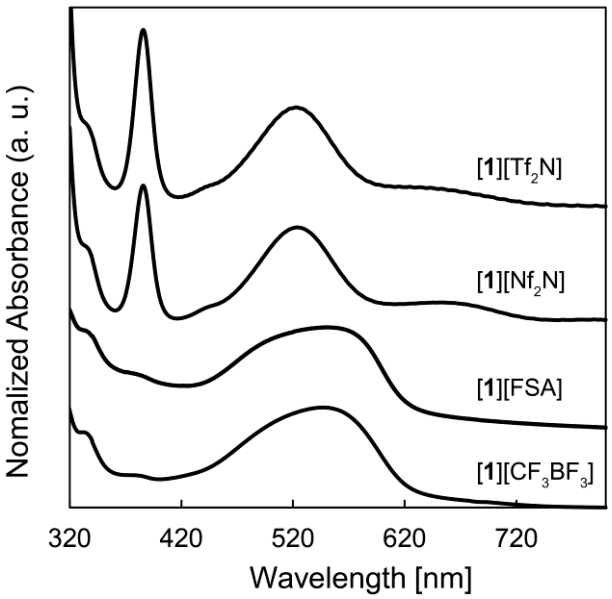

Figure 7. UV-vis spectra of [**1**][Tf_2N] (liquid), [**1**][Nf_2N] (liquid), [**1**][FSA] (solid), and [**1**][CF_3BF_3] (solid) at room temperature. The spectra are normalized based on the absorption band of dimer.

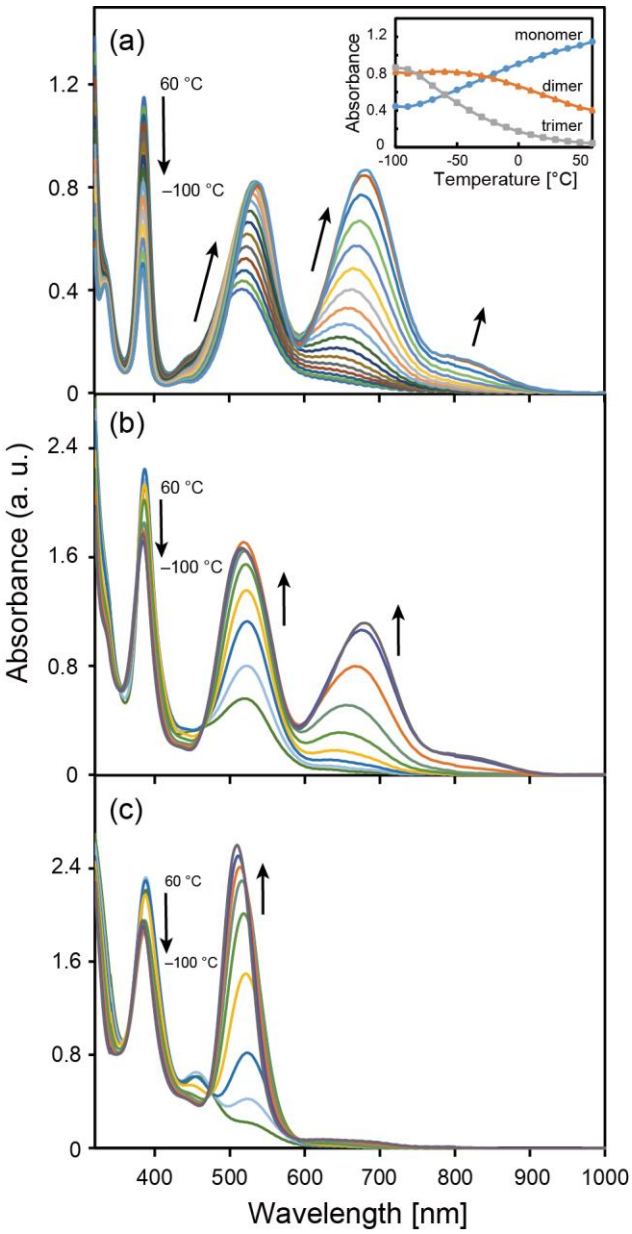

Figure 8. Temperature dependence of the UV-vis spectra of (a) [**1**][Tf_2N], (b) [**1**]$_{0.51}$[**1-MeI**]$_{0.49}$[Tf_2N], and (c) [**1**]$_{0.11}$[**1-MeI**]$_{0.89}$[Tf_2N] recorded during the cooling process. The spectra of [**1**][Tf_2N] and [**1**]$_x$[**1-MeI**]$_{(1-x)}$[Tf_2N] were measured at 10 °C and 20 °C intervals, respectively. Inset in (a) shows the temperature dependence of the absorbance of the monomer (~387 nm), dimer (~520 nm), and trimer (~650 nm) bands.

Luminescence

Rhodium(I) isocyanide complexes exhibit luminescence from their dimers in solutions and in the solid state.[8] [**1**][Tf_2N] exhibited luminescence at approximately 720 nm in the liquid and glassy

states. Consistently, the peak corresponding to the absorption of the dimers was observed at 520 nm in the excitation spectrum.

The temperature dependence of the emission spectra of [**1**][Tf_2N] is shown in Figure 9. The emission intensity was almost constant below the glass transition temperature (T_g = –85 °C), although it gradually decreased above the T_g due to molecular motion and decreased dimer concentration in the liquid state. The emission wavelength was almost constant (717 nm) below the T_g, but exhibited a slight redshift with increasing temperature (to 724 nm at 300 K). The blue-shift of the emission band in the glassy state compared to that of the liquid state can be ascribed to rigidochromism.[8b,14] On the other hand, [**1-MeI**][Tf_2N] was not fluorescent. Therefore, [**1**][Tf_2N] has a (negative) vapoluminescence property when exposed to methyl iodide vapor. The solid [**1**][FSA] also exhibited emission from dimer at 722 nm (Figure S9, supporting information).

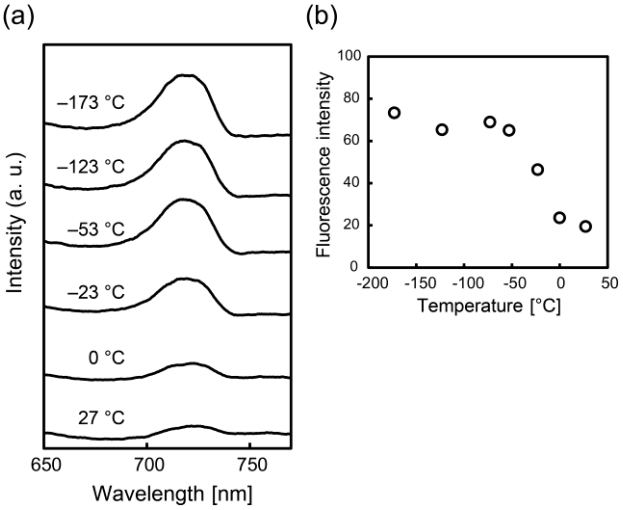

Figure 9. (a) Temperature-dependence of the emission spectra of [**1**][Tf_2N] (excitation wavelength: 525 nm). (b) The temperature dependence of the emission intensity monitored at 722 nm.

Thermal stability

Thermogravimetric analysis (TG) was performed to investigate the thermal decomposition behavior of the prepared ionic liquids. The decomposition temperatures (–3 wt%) of the complexes are listed in Table 1, and their TG curves are shown in Figure S10 (supporting information).

[**1**]X (X = Tf_2N, Nf_2N, FSA, CF_3BF_3) decomposed at approximately 260 °C, where a steep

weight loss due to dissociation of the isocyanide ligands (~ −50 wt%) occurred. Gradual weight loss due to the decomposition of anions occurred at higher temperatures. These isocyanide complexes exhibited much higher thermal stabilities than nitrile complexes such as $[Cu(CH_3CN)_4][Tf_2N]$, which typically decompose at ~70 °C.[3f,15] Isocyanide complexes are organometallic compounds with strong coordination bonds and small effective charges on the metal center, hence they form thermally robust ionic liquids with low melting points.

The decomposition temperature of [**1**-**I**$_2$][Tf_2N] was determined to be 247 °C (–3 wt%). A 60 wt% weight loss was observed at approximately this temperature, which corresponded to the dissociation of both isocyanide and iodide ligands. In contrast to the other salts, the TG curve of [**1**-**MeI**][Tf_2N] exhibited a gradual weight loss above 250 °C. Since the DTA measurement of this salt revealed an exothermic peak at approximately 114 °C (ΔH = 65 kJ mol^{-1}, Figure S11, supporting information), the weight loss corresponds to the decomposition of a reaction product. These results demonstrate that the oxidative adducts do not to return to the square planar complexes by heating.

Viscosity

The temperature dependence of the viscosity of [**1**][Tf_2N] was measured between 50 and −20 °C (Figure 10). The viscosity at room temperature was 121.0 mPa s, and it was a Newtonian fluid. This viscosity was more than two times higher than that of [Bmim][Tf_2N] (49.0 mPa s; Bmim = 1-butyl-3-methylimidazolium cation)[16] and comparable to that of another organometallic ionic liquid, [Ru(C_5H_5)(C_6H_5*n*Bu)][Tf_2N] (136.6 mPa s).[17] [**1**][Tf_2N] had a lower viscosity than an ammonium salt [N($^nC_6H_{13}$)$_4$][Tf_2N] (430 mPa s at 25 °C) with similar substituent length.[18] The parameters obtained by fitting the data with the VFT equation ($\eta = \eta_0 e^{(DT_0/(T-T_0))}$)[19] were $\eta_0 = 6 \times 10^{-3}$ mPa s, T_0 = –181 °C and D = 22, where T_0 is the ideal glass transition temperature. At lower temperatures, the viscosity is expected to rise more rapidly due to the higher concentration of oligomers. Therefore, it seems reasonable that the actual glass transition temperature (T_g = –85 °C) was much higher than the predicted T_0 (–181 °C) obtained by fitting the data above −20 °C.

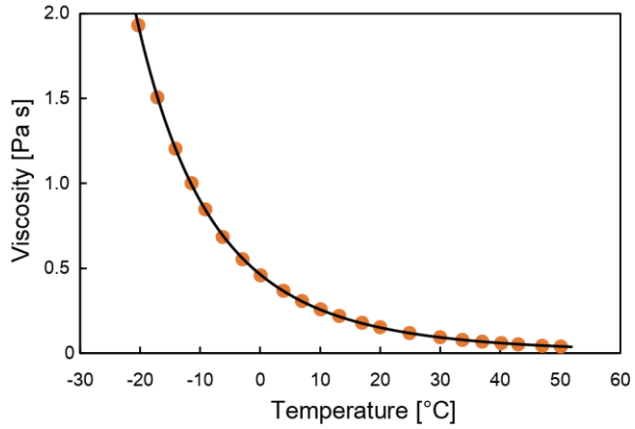

Figure 10. Temperature dependence of the viscosity of [**1**][Tf_2N] (●). Solid line represents the best fit to the VFT equation.

Synthesis and thermal properties of iodine adducts

Oxidative addition of [**1**][Tf_2N] and iodine were performed in dichloromethane solutions, and the resulting products were dependent on the amount of iodine used. Using 1, 1/2, and 1/3 molar equivalents of iodine mainly produced [**1-I₂**][Tf_2N] (brown solid, 34% yield), a dinuclear complex [**2-I₂**][Tf_2N]$_2$ (brown solid, 60% yield), and a trinuclear complex [**3-I₂**][Tf_2N]$_3$ (purple solid, 34% yield), respectively. A similar reaction was reported for other rhodium isocyanide complexes.[20] This result contrasts with the reaction of [**1**][Tf_2N] and MeI, which gave mixtures of [**1**][Tf_2N] and [**1-MeI**][Tf_2N] (vide ante). However, these polynuclear complexes dissociated in chloroform solutions, giving mixtures of [**1**][Tf_2N] and [**1-I₂**][Tf_2N].

The DSC data of the iodine adducts are listed in Table 1 and shown Figure S1 (supporting information). [**1-I₂**][Tf_2N] (T_m = 119.1 °C) exhibited a melting point higher than 100 °C, which is exceptional among the salts synthesized in this study. It exhibited a much higher melting point than [**1-MeI**][Tf_2N] (T_m = 32.2 °C), which can be ascribed to its higher molecular weight, larger volume, and higher symmetry of the cation. Conversely, [**2-I₂**][Tf_2N]$_2$ (T_m = 47.4 °C) and [**3-I₂**][Tf_2N]$_3$ (T_m = 46.4 °C) were ionic liquids with low melting points, despite containing bulky and polyvalent cations. The latter salt exhibited a glass transition temperature of –52 °C on cooling from the melt, and exhibited cold-crystallization upon heating. The ratio of T_g to T_m (T_g/T_m = 0.69) for this salt was

consistent with the empirical rule.[13]

Crystal structures of the iodine adducts

The crystal structures of the [**1-I$_2$**][Tf_2N], dinuclear complex [**2-I$_2$**][Tf_2N]$_2$, and trinuclear complex [**3-I$_2$**][Tf_2N]$_3$ were determined at 100 K. The ORTEP diagrams of these molecules are shown in Figure 11 and their packing diagrams are shown in Figure S12 (supporting information).

The space group of [**1-I$_2$**][Tf_2N] was $P2_1$, and the cation and anion were crystallographically independent (Z = 4). The substituents of the cation exhibited a twisted conformation with two of the four butyl substituents being disordered. The two iodo ligands occupied the *trans* positions and the isocyanide ligands formed a planar coordination plane. The Rh–C (1.983(7)–1.997(7) Å) and Rh–Rh (2.686(1), 2.676(1) Å) bond distances were comparable to those in [Rh(*p*-$MeC_6H_4NC)_4I_2$][TCNQ] (Rh–C = 1.985(7), 1.993(6) Å, Rh–I = 2.677(1) Å).[21] The Tf_2N anion exhibited a *trans* conformation, and the cations and anions arranged alternately in the crystal lattice with no significant intermolecular interactions.

The space group of [**2-I$_2$**][Tf_2N]$_2$ was $P2_1$/n, and the one cation and two anions were crystallographically independent (Z = 4). The cation was composed of a dinuclear complex with a Rh–Rh bond and two axial iodo ligands. The two [Rh(*n*$BuNC)_4$I] units were twisted by 40° from an eclipsed conformation, and the butyl groups extended in the axial direction. The Rh–Rh, Rh–I^1, Rh–I^2 bond distances were 2.7407(6), 2.7383(6), and 2.7385(6) Å, respectively, which are comparable to those in [{Rh(*p*-$CH_3C_6H_4NC)_4$}$_2I_2$][PF_6]$_2$ (Rh–Rh = 2.785(2), Rh–I = 2.735(2) Å).[20a] The two crystallographically independent Tf_2N anions exhibited *cis* and *trans* conformations.

Structural determination of [**3-I$_2$**][Tf_2N]$_3$ was performed at 100 K and the trinuclear structure of the cation is shown in Figure S13 (supporting information), which resembles that of [{Rh$(PhNC)_4$}$_3I_2$][PF_6]$_3$.[20b] However, a detailed discussion of the structure is not possible because the refinements were unsatisfactory due to the low quality of the crystal.

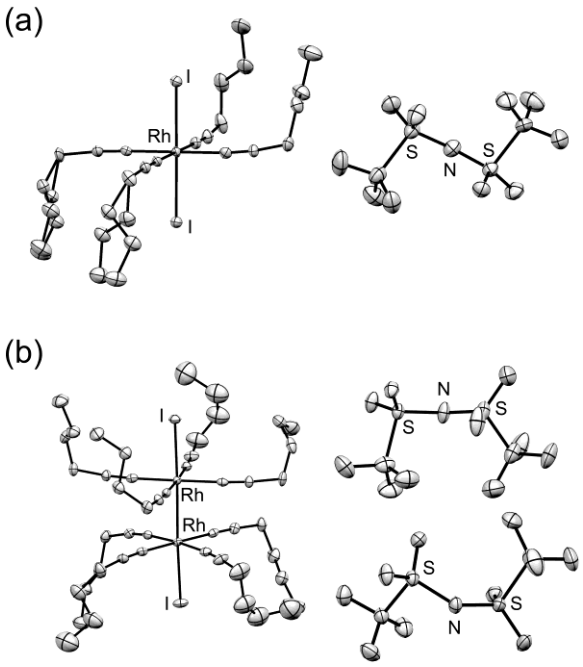

Figure 11. ORTEP drawings of the cation and anion in (a) [**1-I$_2$**][Tf_2N] and (b) [**2-I$_2$**][Tf_2N]$_2$. Hydrogen atoms have been omitted for clarity.

Conclusion

In this study, reactive organometallic ionic liquids containing a Rh(I) isocyanide complex were synthesized. These ionic liquids exhibited thermochromism in the liquid state originating from the Rh–Rh interaction, and the color range was easily controlled by oxidative addition with methyl iodide vapor. The oxidation addition reaction of the Tf_2N salt with iodine produced ionic liquids with dinuclear and trinuclear structures. Furthermore, the Rh(I)-containing ionic liquids exhibited fluorescence from the dimer.

Although a number of thermochromic materials have been reported to date, reports of non-volatile liquid thermochromic materials are scarce. Thermochromic ionic liquids are advantageous for various applications owing to their inherent features of negligible vapor pressures and ionic conductivity. We previously reported thermochromic ionic liquids based on spin crossover and coordination equilibrium,[11] whereas this study demonstrates a novel fabrication method of multifunctional ionic liquids with thermochromic, fluorescent, chemochromic, and reactive

properties. Addition of various functionalities to ionic liquids using reactive organometallic compounds has the potential to lead to various future applications.

Experimental

General

^{1}H NMR spectra were recorded using a Bruker Avance 400 instrument. The IR spectra were measured using a Thermo Scientific Nicolet iS 5 FT-IR attached with an ATR unit (diamond) or JASCO FT/IR-4700. UV-vis spectra were measured using a JASCO V-570 UV/VIS/NIR spectrophotometer. Measurements of the solid and liquid samples were performed using KBr plates and alkoxysilane-coated quartz plates, respectively. Variable temperature measurements were performed using a UNISOKU cryostat CoolSpeK UV USP-203-A or a Linkam hot stage LTSE-350. Luminescence emission spectra were measured using a JASCO FP-6600. DSC measurements were performed using a TA Q100 differential scanning calorimeter at a scan rate of 10 K min^{-1}, with other rates applied as required. The viscosities of the liquids were measured using a Toki Sangyo TV-22L viscometer equipped with a 3 R7.7 cone rotor.

Syntheses of [Rh(*n*BuNC)$_4$]X ([1]X; X = Tf$_2$N, Nf$_2$N, FSA, CF$_3$BF$_3$)

[1][Tf$_2$N]. Under a nitrogen atmosphere, *n*BuNC (0.105 mL, 0.8 mmol) was added dropwise to a suspension of [Rh(C_8H_{12})Cl]$_2$ (100 mg, 0.20 mmol) in methanol (4 mL) with stirring. When the solution turned red, a methanol solution of K[Tf$_2$N] (52.8 mg, 0.3 mmol) was added dropwise and stirred. Then, the solvent was removed under vacuum, and the residue was dissolved in CH_2Cl_2. The subsequently precipitated white powder was removed by filtration, and the filtrate was evaporated under reduced pressure. The resultant oil was again dissolved in CH_2Cl_2, and the solution was washed with water (2 mL, 3 times). The solution was dried over anhydrous $MgSO_4$ and then washed with hexane (2 mL, 3 times). Evaporation of the solvent under reduced pressure resulted in the formation of an oil, which was dried under vacuum for 1 h at room temperature, to yield the desired product as

a purple liquid (221 mg, 77%). ^{1}H NMR (400 MHz, $CDCl_3$): δ = 0.98 (t, 3H, -CH_3, J = 7.6 Hz), 1.48 (m, 2H, -CH_2CH_3), 1.75 (m, 2H, -$CH_2C_2H_5$), 3.71 ppm (t, 2H, -$CH_2C_3H_7$, J = 6.8 Hz); elemental analysis calcd (%) for $C_{22}H_{36}N_5O_4F_6S_2Rh$: C 36.93, H 5.07, N 9.79; found: C 36.65, H 4.76, N 9.76.

[1][Nf$_2$N]. This salt was prepared according to the procedure described for [**1**][Tf$_2$N], but using [Rh(C_8H_{12})Cl]$_2$ (100 mg, 0.20 mmol), MeOH (3 mL), *n*BuNC (0.17 mL, 1.6 mmol), and Li[Nf$_2$N] (478 mg, 0.82 mmol) as precursors. A small amount of CH_2Cl_2 was added to the methanol solution of the product, and the solution was left at –40 °C for 1 h. A white powder was precipitated and removed by filtration and the solvent was evaporated under reduced pressure from the filtrate. The resultant oil was dissolved in a small amount of ethanol and cooled to –40 °C, resulting in the precipitation of a red-purple powder. The solvent was then removed by decantation. The resultant powder was recrystallized from ethanol, and the solvent was subsequently removed by decantation. The powder was washed twice with cold ethanol at –40 °C. The solvent was then removed by drying under vacuum for 4 h at 40 °C to yield the desired product as a purple liquid (255 mg, 62%). ^{1}H NMR (400 MHz, $CDCl_3$): δ = 0.97 (t, 3H, -CH_3, J = 7.6 Hz), 1.48 (m, 2H, -CH_2CH_3), 1.75 (m, 2H, -$CH_2C_2H_5$), 3.70 ppm (t, 2H, -$CH_2C_3H_7$, J = 6.8 Hz). elemental analysis calcd (%) for $C_{28}H_{36}N_5F_{18}RhS_2$: C 33.11, H 3.57, N 6.90; found: C 33.12, H 3.55, N 6.97.

[1][FSA]. This salt was prepared according to the procedure described for [**1**][Nf$_2$N], but using [Rh(C_8H_{12})Cl]$_2$ (100 mg, 0.20 mmol), MeOH (4 mL), *n*BuNC (0.24 mL, 1.8 mmol), and K[FSA] (132 mg, 0.60 mmol). A small amount of ether was added instead of CH_2Cl_2 to the obtained methanol solution of the product. Recrystallization from ethanol yielded the desired product as purple crystals (105 mg, 43%). Evaporation of the solvent from the filtrate under reduced pressure, followed by recrystallization from ethanol resulted in a second crop (82 mg, 33%). The samples were recrystallized twice from ethanol and then used for physical measurements. ^{1}H NMR (400 MHz, $CDCl_3$): δ = 0.98 (t, 3H, -CH_3, J = 7.6 Hz), 1.48 (m, 2H, -CH_2CH_3), 1.76 (m, 2H, -$CH_2C_2H_5$), 3.71 ppm (t, 2H, -$CH_2C_3H_7$, J = 6.8 Hz); elemental analysis calcd (%) for $C_{20}H_{36}N_5O_4F_2S_2Rh$: C 39.02, H 5.90, N 11.38; found: C 39.02, H 5.80, N 11.42.

[1][CF_3BF_3]. This salt was prepared according to the procedure described for [**1**][Nf_2N], but using [$Rh(C_8H_{12})Cl]_2$ (50 mg, 0.10 mmol), MeOH (6 mL), *n*BuNC (0.105 mL, 0.80 mmol), and K[CF_3BF_3] (53 mg, 0.30 mmol). The desired product was obtained as purple needle crystals (78 mg, 68%). ^{1}H NMR (400 MHz, $CDCl_3$): δ = 0.98 (t, 3H, -CH_3, *J* = 7.2 Hz), 1.48 (m, 2H, -CH_2CH_3), 1.75 (m, 2H, -$CH_2C_2H_5$), 3.71 (t, 2H, -$CH_2C_3H_7$, *J* = 6.8 Hz); elemental analysis calcd (%) for $C_{21}H_{36}N_4BF_6Rh$: C, 44.08; H, 6.34; N, 9.79. Found: C, 44.18; H, 6.17; N, 9.81.

Synthesis of the oxidative adducts

[Rh(*n*BuNC)$_4$MeI][Tf_2N] ([1-MeI][Tf_2N]). Methyl iodide (0.327 mL, 5.26 mmol) was added dropwise to a solution of [**1**][Tf_2N] (188 mg, 0.26 mmol) in CH_2Cl_2 (5 mL) with stirring. The solution was stirred under a nitrogen atmosphere for 1 d. The solvent was then removed under vacuum, and the resultant oil was dissolved in ethanol. The solution was left at –40 °C to precipitate a pale yellow powder. The powder was collected by filtration and dried under vacuum to yield the desired product (34%). ^{1}H NMR (400 MHz, $CDCl_3$): δ = 1.00 (t, 3H, -CH_2CH_3, *J* = 7.2 Hz), 1.29 (s, 3H, Rh-CH_3), 1.51 (m, 2H, -CH_2CH_3), 1.81 (m, 2H, -$CH_2C_2H_5$), 3.89 ppm (t, 2H, -$CH_2C_3H_7$, *J* = 6.8 Hz); IR (ATR): ν = 570, 600, 616, 653, 739, 761, 786, 922, 1056, 1135, 1181, 1226, 1349, 1464, 2235 (NC), 2876, 2962, 2960 cm^{-1}; elemental analysis calcd (%) for $C_{23}H_{39}F_6IN_5O_4RhS_2$: C 32.22, H 4.58, N 8.17; found: C 32.32, H 4.85, N 8.12. This salt was readily obtained by the reaction of [**1**][Tf_2N] and methyl iodide vapor. The mixtures of [**1**][Tf_2N] and [**1-MeI**][Tf_2N] used for the thermochromism experiments were prepared by placing [**1**][Tf_2N] under the methyl iodide vapor in a closed petri dish for an appropriate amount of time. Then, the samples were left in air for 2 h to ensure evaporation of any unreacted methyl iodide. The ratio of [**1**][Tf_2N] and [**1-MeI**][Tf_2N] in the samples were determined by ^{1}H NMR.

[Rh(*n*BuNC)$_4$I$_2$][Tf_2N] ([1-I$_2$][Tf_2N]). A solution of [**1**][Tf_2N] (32.8 mg, 0.046 mmol) in CH_2Cl_2 (3 mL) was added dropwise to a solution of iodine (11 mg, 0.042 mmol) in CH_2Cl_2 with stirring. The color of the solution immediately turned from orange to red, and the solution was subsequently stirred

for 9 h under a nitrogen atmosphere. The solvent was removed under vacuum, and the resultant oil was dissolved in ethanol, which was then left at –40 °C to precipitate a brown powder. The powder was collected by filtration and dried under vacuum to yield the desired product (10.6 mg, 23%). ^{1}H NMR (400 MHz, $CDCl_3$): δ = 1.01 (t, 3H, -CH_3, J = 7.2 Hz), 1.56 (m, 2H, -CH_2CH_3), 1.85 (m, 2H, -$CH_2C_2H_5$), 4.04 ppm (t, 2H, -$CH_2C_3H_7$, J = 6.8 Hz); IR (ATR): ν = 532, 555, 567, 616, 655, 739, 789, 841, 919, 1057, 1138, 1180, 1225, 1350, 1439, 2251 (NC), 2873, 2932, 2960 cm^{-1}; elemental analysis calcd (%) for $C_{22}H_{36}F_6I_2N_5O_4RhS_2$: C 27.26, H 3.74, N 7.22; found: C 27.39, H 3.76, N 7.18.

[{Rh(*n*BuNC)$_4$}$_2$I$_2$][Tf$_2$N]$_2$ ([2-I$_2$][Tf$_2$N]$_2$). [**1**][Tf_2N] (17.5 mg, 0.025 mmol) and iodine (2.9 mg, 0.11 mmol) were dissolved in ethanol (2 mL), and the solution was left at –40 °C for 1 day to precipitate brown plate crystals. The crystals were collected by filtration and dried under vacuum for 3 h at room temperature to yield the desired product (11.5 mg, 60%). A solution of the complex in chloroform-*d* gave a ^{1}H NMR spectrum indicating a 1:1 mixture of [**1**][Tf_2N] and [**1**-**I$_2$**][Tf_2N].[20a] ^{1}H NMR (400 MHz, $CDCl_3$): δ = 1.00 (m, 24H, -CH_3, J = 7.2 Hz), 1.51 (m, 16H, -CH_2CH_3), 1.75 (m, 8H, -$CH_2C_2H_5$), 1.85 (m, 8H, -$CH_2C_2H_5$), 3.70 (t, 8H, -$CH_2C_3H_7$, J = 6.8 Hz), 4.04 ppm (t, 8H, -$CH_2C_3H_7$, J = 6.4 Hz); IR (ATR): ν = 554, 570, 598, 618, 652, 739, 762, 787, 923, 947, 1053, 1131, 1179, 1223, 1344, 1451, 2226 (NC), 2876, 2935, 2961 cm^{-1}; elemental analysis calcd (%) for $C_{44}H_{72}F_{12}I_2N_{10}O_8Rh_2S_4$: C 31.36, H 4.31, N 8.31; found: C 31.46, H 3.87, N 8.30.

[{Rh(*n*BuNC)$_4$}$_3$I$_2$][Tf$_2$N]$_3$ ([3-I$_2$][Tf$_2$N]$_3$). [**1**][Tf_2N] (57.5 mg, 0.080 mmol) and iodine (6.8 mg, 0.27 mmol) were dissolved in ethanol (2 mL), and the solution was left at –40 °C for 1 day. The precipitated powder was collected by filtration and dried in air. The powder was then dissolved in ethanol and slowly cooled to –40 °C. Red purple plate crystals were precipitated in 1 day, and were collected by filtration and dried under vacuum for 3 h at room temperature to yield the desired product (21.6 mg, 34%). A solution of the complex in chloroform-*d* gave a ^{1}H NMR spectrum indicating a 2:1 mixture of [**1**][Tf_2N] and [**1**-**I$_2$**][Tf_2N]. ^{1}H NMR (400 MHz, $CDCl_3$): δ = 1.00 (m, 36H, -CH_3, J = 7.2 Hz), 1.51 (m, 24H, -CH_2CH_3), 1.75 (m, 16H, -$CH_2C_2H_5$), 1.85 (m, 8H, -$CH_2C_2H_5$), 3.71 (t, 16H, -$CH_2C_3H_7$, J = 6.8 Hz), 4.04 ppm (t, 8H, -$CH_2C_3H_7$, J = 6.4 Hz); IR (ATR): ν = 535, 548, 570, 610,

655, 739, 762, 789, 923, 1053, 1136, 1183, 1226, 1345, 1439, 2214 (NC), 2876, 2963 cm^{-1}; elemental analysis calcd (%) for $C_{66}H_{108}F_{18}I_2N_{15}O_{12}Rh_3S_6$: C 33.02, H 4.53, N 8.75; found: C 32.94, H 4.18, N 8.72.

X-ray crystallography

Single crystals of [**1**-$\mathbf{I_2}$][Tf_2N] and [**2**-$\mathbf{I_2}$][Tf_2N]$_2$ for X-ray crystallography were grown by slow cooling of their respective ethanol solutions to –40 °C. The X-ray diffraction data were collected using a Bruker APEX II Ultra CCD diffractometer with Mo Kα radiation at 100 K. The crystallographic parameters are listed in Table S1 (supporting information). The structures were solved by the intrinsic phasing method and refined using SHELXL[22] and mercury was used to generate the molecular graphics.[23] The occupancies of two alkyl chains disordered in the cation of [**1**-$\mathbf{I_2}$][Tf_2N] were 0.50:0.50 and 0.65:0.35. We also performed structural determination of [**3**-$\mathbf{I_2}$][Tf_2N]$_3$ at 100 K, but refinements were unsatisfactory because of the low quality of the crystal. CCDC-1584845 ([**1**-$\mathbf{I_2}$][Tf_2N]) and -1588725 ([**2**-$\mathbf{I_2}$][Tf_2N]$_2$) contain the supplementary crystallographic data for this paper. These data are provided free of charge by The Cambridge Crystallographic Data Centre.

Acknowledgments

We thank Prof. T. Uchino (Kobe University) for his help with the fluorescent measurements. This work was financially supported by KAKENHI (grant number 16H04132) from the Japan Society for the Promotion of Science (JSPS).

[1] A. Stark, K. R. Seddon, in Kirk-Othmer Encyclopedia of Chemical Technology, *vol. 26*, Wiley-Interscience, New York, 5th ed., **2007**, pp. 836–919.

[2] a) Y. Yoshida, G. Saito, in Ionic Liquids: Theory, Properties, New Approaches, ed. A. Kokorin, InTech, **2011**; b) R. E. Del Sesto, C. Corley, A. Robertson, J. Wilkes, *J. Organomet. Chem.* **2005**, *690*, 2536–2542; c) A. Branco, L. C. Branco, F. Pina, *Chem. Commun.* **2011**, *47*, 2300–2302; d) P. Zhang, Y. Gong, Y. Lv, Y. Guo, Y. Wang, C. Wang, H. Li, *Chem. Commun.* **2012**, *48*, 2334–2336; e) P. Nockemann, B. Thijs, N. Postelmans, K. Van Hecke, L. Van Meervelt, K. Binnemans, *J. Am. Chem. Soc.* **2006**, *128*, 13658–13659; f) B. Mallick, B. Balke, C. Felser, A.-V. Mudring, *Angew. Chem., Int. Ed.* **2008**, *47*, 7635–7638; g) R. J. C. Brown, P. J. Dyson, D. J. Ellis, T. Welton, *Chem. Commun*. **2001**, *3*, 1862–1863.

[3] a) H. Masui, R. W. Murray, *Inorg. Chem.* **1997**, *36*, 5118–5126; b) I. J. B. Lin, C. S. Vasam, *J. Organomet. Chem.* **2005**, *690*, 3498–3512; c) J. F. Huang, H. M. Luo, S. Dai, *J. Electrochem. Soc.* **2006**, *153*, J9–J13; d) M. Iida, C. Baba, M. Inoue, H. Yoshida, E. Taguchi, H. Furusho, *Chem. Eur. J.* **2008**, *14*, 5047–5056; e) H. D. Pratt III, A. J. Rose, C. L. Staiger, D. Ingersoll, T. M. Anderson, *Dalton Trans.* **2011**, *40*, 11396–11401; f) N. R. Brooks, S. Schaltin, K. Van Hecke, L. Van Meervelt, K. Binnemans, J. Fransaer, *Chem. Eur. J.* **2011**, *17*, 5054–5059.

[4] a) T. Inagaki, T. Mochida, M. Takahashi, C. Kanadani, T. Saito and D. Kuwahara, *Chem. Eur. J.* **2012**, *18*, 6795–6804; b) Y. Funasako, T. Inagaki, T. Mochida, T. Sakurai, H. Ohta, K. Furukawa and T. Nakamura, *Dalton Trans.* **2013**, *42*, 8317–8327; c) Y. Funasako, S. Mori and T. Mochida, *Chem. Commun.* **2016**, *52*, 6277–6279; d) Y. Funasako, T. Mochida, K. Takahashi, T. Sakurai and H. Ohta, *Chem. Eur. J.* **2012**, *18*, 11929–11936.

[5] a) K. R. Mann, N. S. Lewis, R. M. Williams, H. B. Gray, J. G. Gordon, *Inorg. Chem.* **1978**, *17*, 828–834; b) N. T. Tran, J. R. Stork, D. Pham, C. J. Chancellor, M. M. Olmstead, J. C. Fettinger, A. L. Balch, *Inorg. Chem.* **2007**, *46*, 7998–8007.

[6] A. K. Chan, K. M. Wong, V. W. Yam, *J. Am. Chem. Soc*. **2015**, *137*, 6920–6931.

[7] L. T. Lo, W. Chu, Chun. Tam, S. Yiu, Chi. Ko, S. Chiu, *Organometallics* **2011**, *30*, 5873–5881.

[8] a) V. M. Miskowski, G. L. Nobinger, D. S. Kliger, G. S. Hammond, N. S. Lewis, K. R. Mann, H. B. Gray, *J. Am. Chem. Soc.* **1978**, *100*, 485–488; b) V. M. Miskowski, S. F. Rice, H. B. Gray, R. F. Dallinger, S. J. Milder, M. G. Hill, C. L. Exstrom, K. R. Mann, *Inorg. Chem.* **1994**, *33*, 2799–2807.

[9] a) P. R. Branson, M. Green, *J. Chem. Soc., Dalton Trans.* **1972**, 1303–1310; b) J. A. McCleverty, J. Williams, *Trans. Met. Chem.* **1978**, *3*, 205–211.

[10] a) S. Tang, A. Babai, A.-V. Mudring, *Angew. Chem., Int. Ed.* **2008**, *47*, 7631–7634; b) S. Pitula, A.-V. Mudring, *Chem. Eur. J.* **2010**, *16*, 3355–3365; c) S. Gago, L. Cabrita, J. C. Lima, L. C. Branco, F. Pina, *Dalton Trans.* **2013**, *42*, 6213–6218; d) E. T. Spielberg, E. Edengeiser, B. Mallick, M. Havenith, A.-V. Mudring, *Chem. Eur. J.* **2014**, *20*, 5338–5345; e) A. Tokarev, J. Larionova, Y. Guari,

J. M. López-de-Luzuriaga, M. Monge, P. Dieudonné, C. Blanc, *Dalton Trans.* **2010**, *39*, 10574–10576; f) Y. Yoshida, J. Fujii, G. Saito, T. Hiramatsu, N. Sato, *J. Mater. Chem.* **2006**, *16*, 724; g) Z. -P. Wang, J. -Y. Wang, J.-R. Li, M. -L. Feng, G.-D. Zou, X. -Y. Huang, *Chem. Commun.* **2015**, *51*, 3094–3097; h) T. Ogawa, M. Yoshida, H. Ohara, A. Kobayashi, M. Kato, *Chem. Commun*. **2015**, *51*, 13377–13380.

[11] a) M. Okuhata, Y. Funasako, K. Takahashi, T. Mochida, *Chem. Commun.* **2013**, *49*, 7662–7664; b) X. Lan, T. Mochida, Y. Funasako, K. Takahashi, T. Sakurai, H. Ohta, *Chem. Eur. J.* **2017**, *23*, 823–831.

[12] a) Y. Kohno, M. G. Cowan, M. Masuda, I. Bhowmick, M. P. Shores, D. L. Gin, R. D. Noble, *Chem. Commun.* **2014**, *50*, 6633–6636; b) N. Aoyagi, K. Shimojo, N. R. Brooks, R. Nagaishi, H. Naganawa, K. Van Hecke, L. V. Meervelt, K. Binnemans, T. Kimura, *Chem. Commun.* **2011**, *47*, 4490–4492; c) S. J. Osborne, S. Wellens, C. Ward, S. Felton, R. M. Bowman, K. Binnemans, M. Swadzba-Kwasny, H. Q. N. Gunaratne, P. Nockemann, *Dalton Trans.* **2015**, *44*, 11286−11289; d) X. Wei, L. Yu, D. Wang, X. Jin, G. Z. Chen, *Green Chem.* **2008**, *10*, 296–305; e) B. Monteiro, M. Outis, H. Cruz, J. P. Leal, C. A. T. Laia, C. C. L. Pereira, *Chem. Commun.* **2017**, *53*, 850–853.

[13] a) D. Turnbull and M. H. Cohen, Modern Aspect of the Vitreous State, *vol. 1*, Butterworth, London, **1960**, p. 38; b) O. Yamamuro, Y. Minamimoto, Y. Inamura, S. Hayashi, H. Hamaguchi, *Chem. Phys. Lett.* **2006**, *423*, 371–375.

[14] P. Chen, T. J. Meyer, *Chem. Rev.* **1998**, *98*, 1439–1477.

[15] S. Schaltin, N. R. Brooks, L. Stappers, K. V. Hecke, L. V. Meervelt, K. Binnemans, J. Fransaer, *Phys. Chem. Chem. Phys.* **2012**, *14*, 1706–1715.

[16] a) A. Paul, A. J. Samanta, *J. Phys. Chem. B* **2008**, *112*, 16626–16632; b) H. Tokuda, K. Ishii, M. A. B. H. Susan, S. Tsuzuki, K. Hayamizu, M. Watanabe, *J. Phys. Chem. B* **2006**, *110*, 2833–2839.

[17] A. Komurasaki, Y. Funasako, T. Mochida, *Dalton. Trans.* **2015**, *44*, 7595–7605.

[18] H. Matsumoto, H. Kageyama, Y. Miyazaki, *Chem. Lett*. **2001**, *2*, 182–183.

[19] G. S. Fulcher, *J. Am. Ceram. Soc.* **1925**, *8*, 339–355.

[20] a) M. M. Olmstead, A. L. Balch, *J. Organomet. Chem.* **1978**, *148*, C15–C18; b) A. L. Balch, M. M. Olmstead, *J. Am. Chem. Soc.* **1976**, *98*, 2354–2356; c) A. L. Balch, M. M. Olmstead, *J. Am. Chem. Soc.* **1979**, *101*, 3128–3129.

[21] G. Matsubayashi, T. Iizuma, T. Tanaka, *Inorg. Chim. Acta* **1985**, *102*, 145–150.

[22] a) G. M. Sheldrick, *Acta Cryst.* **2008**, *A64*, 112−122; b) G. M. Sheldrick, *Acta Cryst*. **2015**, *A71*, 3–8; c) G. M. Sheldrick, *Acta Cryst.* **2015**, *C71*, 3–8.

[23] C. F. Macrae, I. J. Bruno, J. A. Chisholm, P. R. Edgington, P. McCabe, E. Pidcock, L. Rodriguez-Monge, R. Taylor, J. van de Streek, P. A. Wood, *J. Appl. Cryst.* **2008**, *41*, 466–470.

Entry for the Table of Contents (Please choose one layout)

Layout 1:

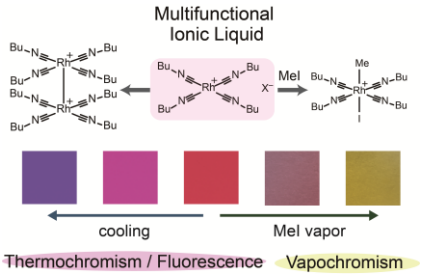

Multifunctional ionic liquids have been designed based on the unique chemical reactivities of organometallic rhodium complexes. The liquids exhibited thermochromism and fluorescence, and the color was tunable by exposure to methyl iodide vapor.

(a)

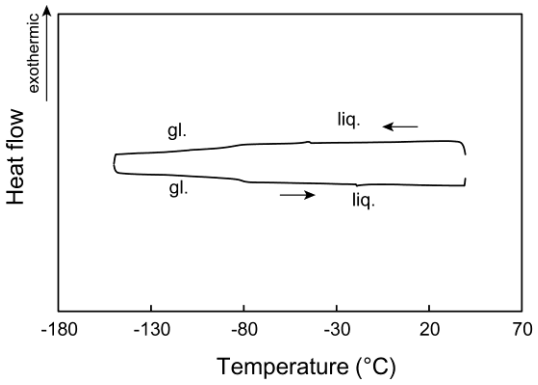
exothermic
Heat flow
gl.
liq.
gl.
liq.
-180
-130
-80
-30
20
70
Temperature (°C)

(b)

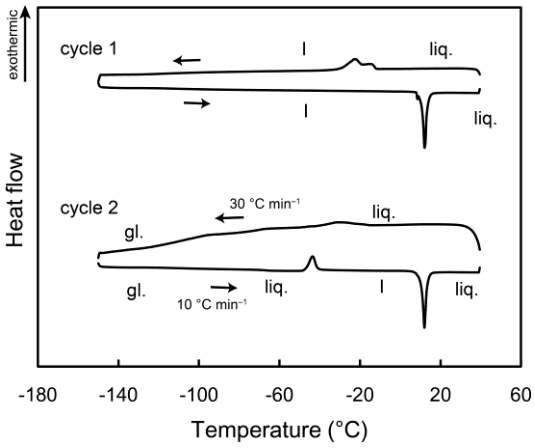
exothermic
cycle 1
I
liq.
I
liq.
Heat flow
cycle 2
30 °C min⁻¹
liq.
gl.
gl.
liq.
10 °C min⁻¹
I
liq.
-180
-140
-100
-60
-20
20
60
Temperature (°C)

(c)

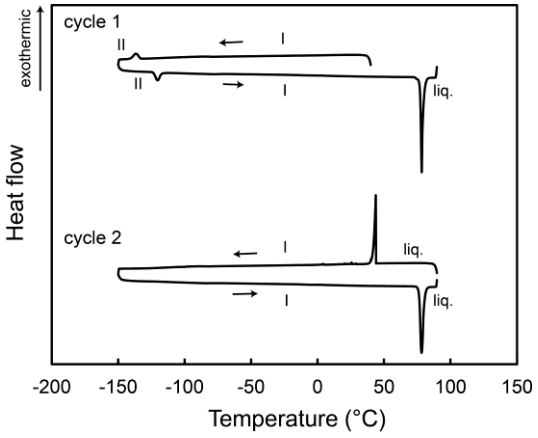
exothermic
cycle 1
II
I
II
I
liq.
Heat flow
cycle 2
I
liq.
I
liq.
-200
-150
-100
-50
0
50
100
150
Temperature (°C)

(d)

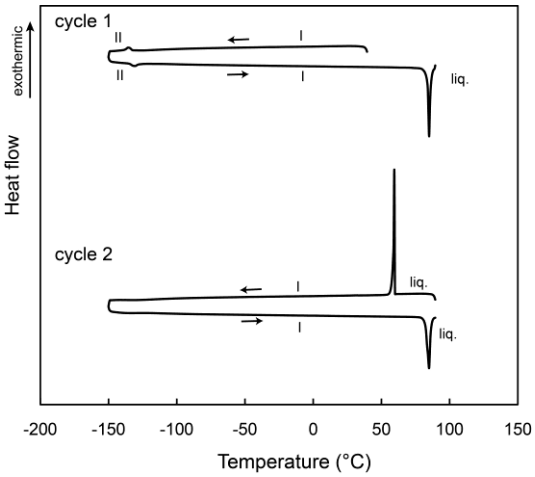
exothermic
cycle 1
II
I
II
I
liq.
Heat flow
cycle 2
I
liq.
I
liq.
-200
-150
-100
-50
0
50
100
150
Temperature (°C)

(e)

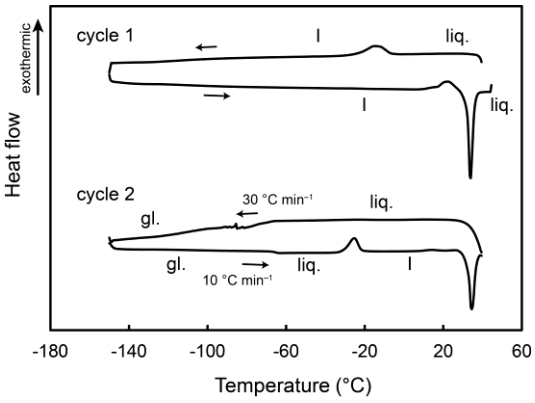
exothermic
cycle 1
I
liq.
I
liq.
Heat flow
cycle 2
30 °C min⁻¹
liq.
gl.
gl.
liq.
10 °C min⁻¹
I
-180
-140
-100
-60
-20
20
60
Temperature (°C)

(f)

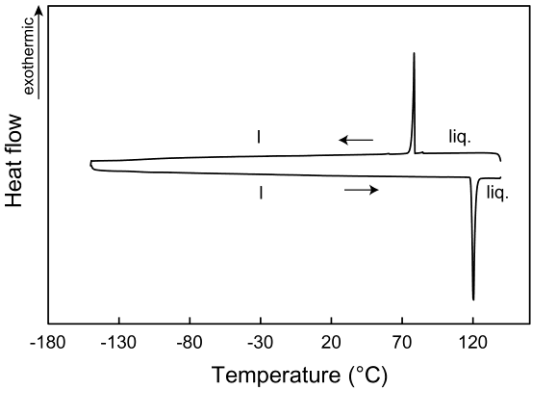
exothermic
I
liq.
I
liq.
Heat flow
-180
-130
-80
-30
20
70
120
Temperature (°C)

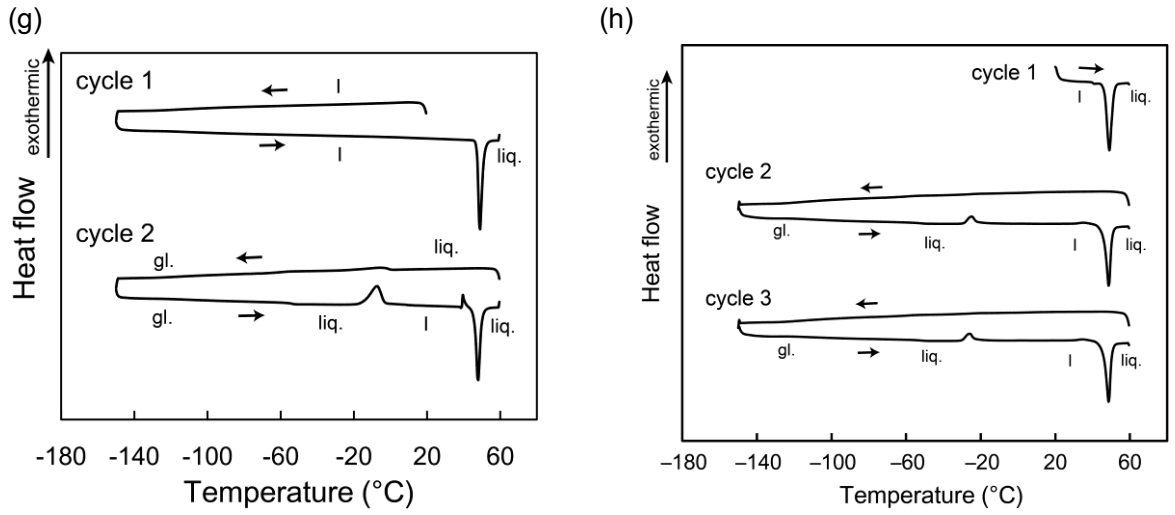

Figure S1. DSC traces of (a) [**1**][Tf_2N], (b) [**1**][Nf_2N], (c) [**1**][FSA], (d) [**1**][CF_3BF_3], (e) [**1-MeI**][Tf_2N], (f) [**1-I$_2$**][Tf_2N], (g) [**2-I$_2$**][Tf_2N], and (h) [**3-I$_2$**][Tf_2N] (I and II: solid phase, *liq.*: liquid phase, *gl.*: glassy phase).

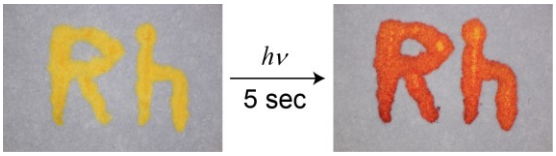

Figure S2. Photographs of [**1-MeI**][Tf_2N] in the liquid state before and after UV photoirradiation for 5 s.

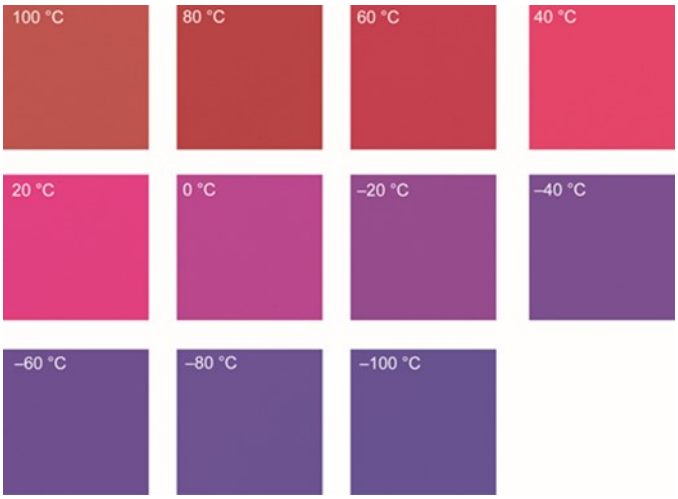

Figure S3. Thermochromism of [**1**][Tf_2N] observed under a microscope. The liquid was sandwiched between quartz plates.

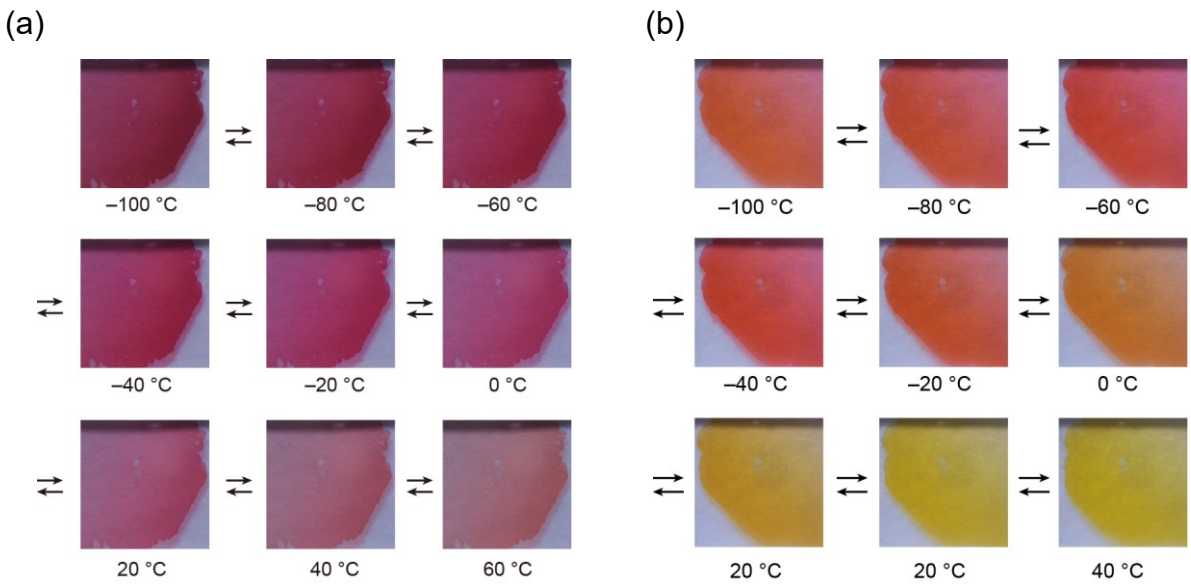

Figure S4. Photographs of the liquid sandwiched between quartz plates demonstrating the thermochromism of $[\mathbf{1}]_x[\mathbf{1\text{-}MeI}]_{(1-x)}[Tf_2N]$ (x = 0.35 (a), 0.03 (b)).

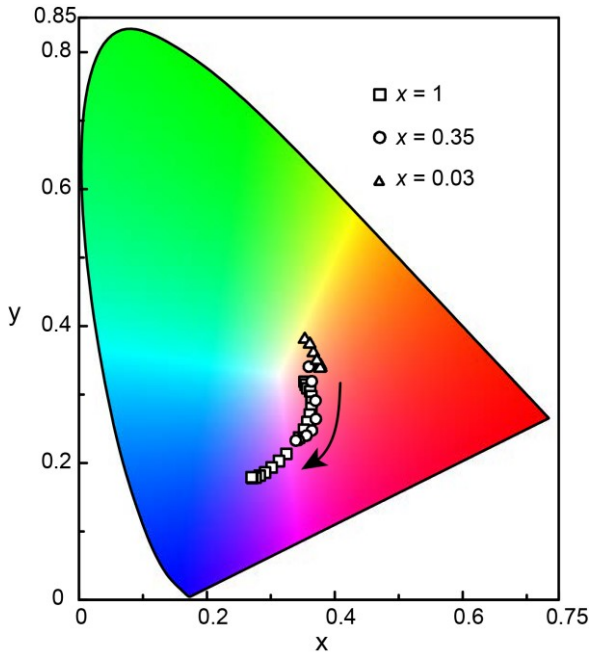

Figure S5. Thermochromic range of $[\mathbf{1}]_x[\mathbf{1\text{-}MeI}]_{1-x}[Tf_2N]$ (x = 1 (□), 0.35 (○), 0.03 (△)) between −100 and 60 °C displayed in xyY color space. The arrow indicates direction of color change upon cooling.

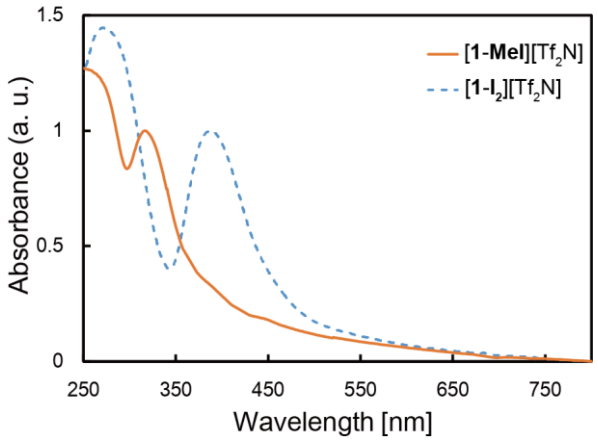

Figure S6. UV-vis spectra of [**1-MeI**][Tf_2N] and [**1-I_2**][Tf_2N] in the solid state measured at room temperature.

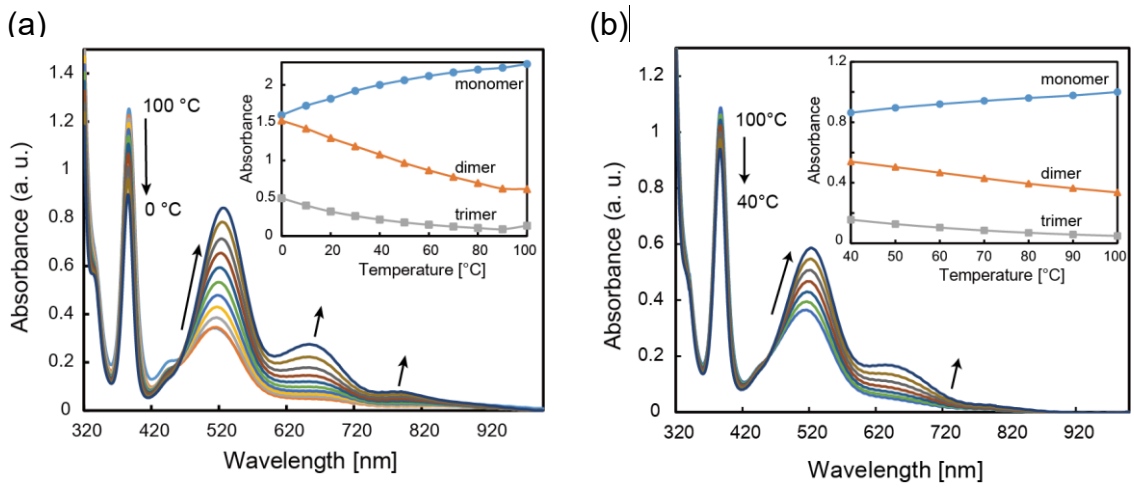

Figure S7. Temperature dependence of the UV-vis spectra of (a) [**1**][Nf_2N] and (b) [**1**][FSA] measured at 10 °C intervals during the cooling process. Inset shows the temperature dependence of the absorbance of the monomer (~387 nm), dimer (~520 nm), and trimer (~650 nm) bands.

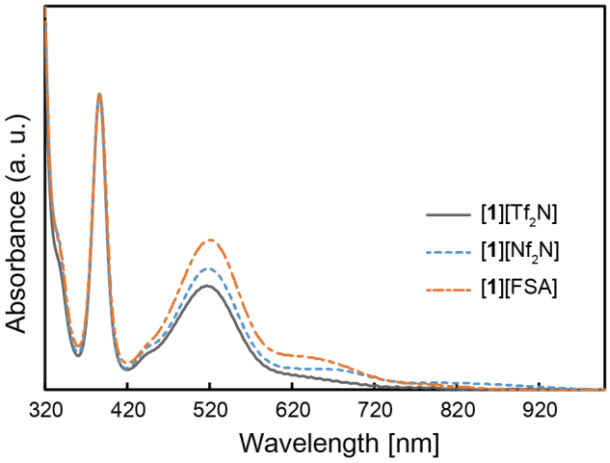

Figure S8. UV-vis spectra of [**1**][Tf_2N], [**1**][Nf_2N], and [**1**][FSA] at 60 °C. The spectra are normalized based on the peak of monomer at 387 nm.

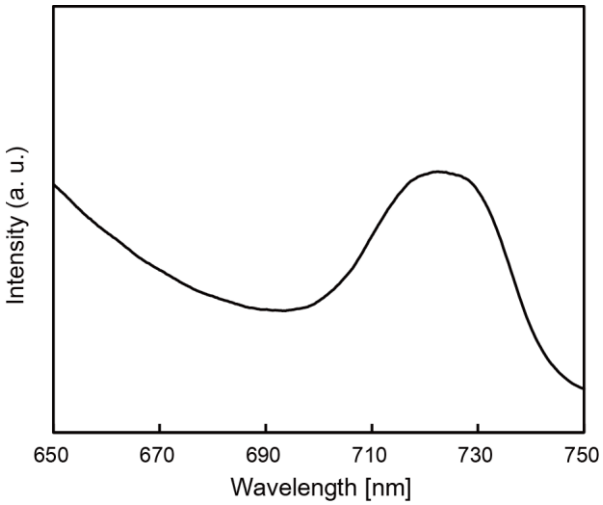

Figure S9. Fluorescence spectrum of [**1**][FSA] in the solid state measured at room temperature (excitation wavelength: 520 nm).

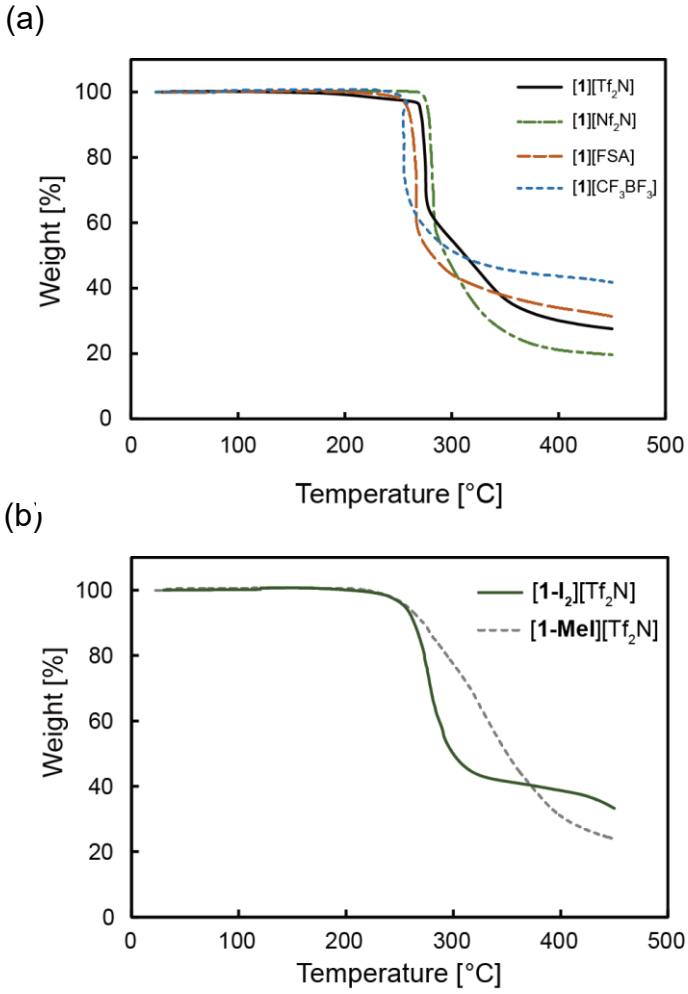

Figure S10. TG curves of (a) [**1**]X (X = Tf_2N, FSA, CF_3BF_3, Nf_2N) and (b) [**1-I$_2$**][Tf_2N] and [**1-MeI**][Tf_2N] measured at 10 $Kmin^{-1}$ under a nitrogen atmosphere.

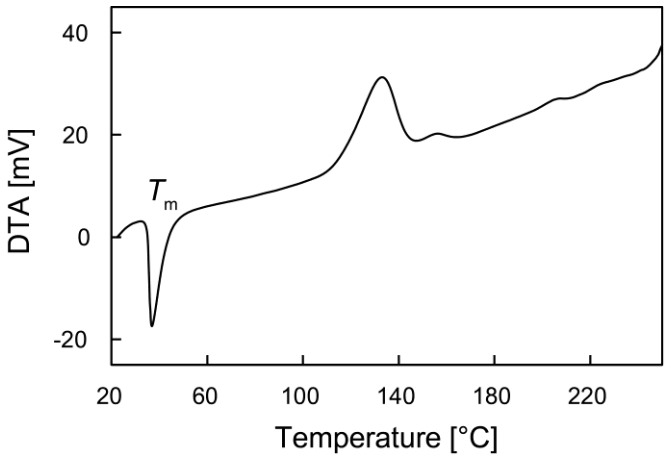

Figure S11. DTA trace of [**1-MeI**][Tf_2N].

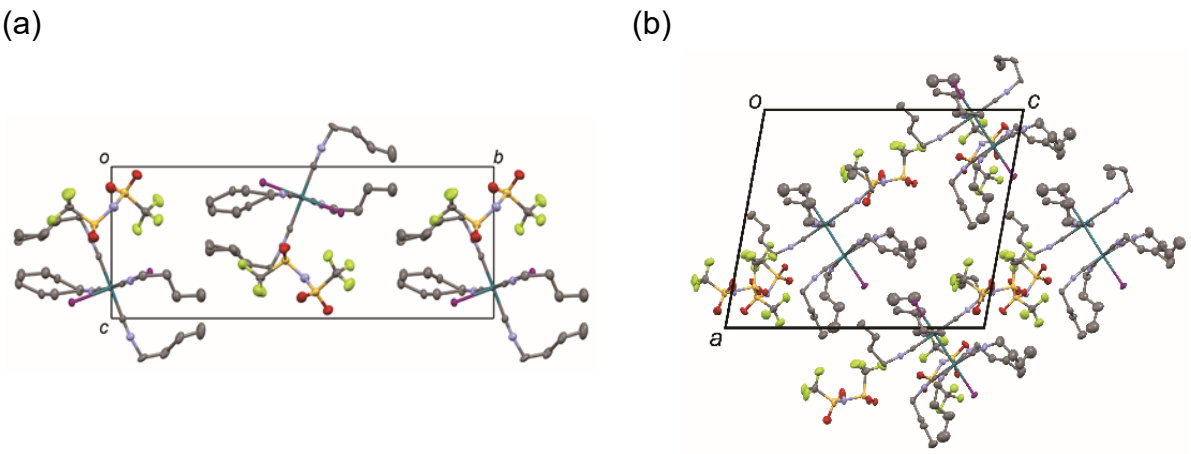

Figure S12. Packing diagrams of (a) [**1-I$_2$**][Tf_2N] and (b) [**2-I$_2$**][Tf_2N]$_2$. Hydrogen atoms have been omitted for clarity.

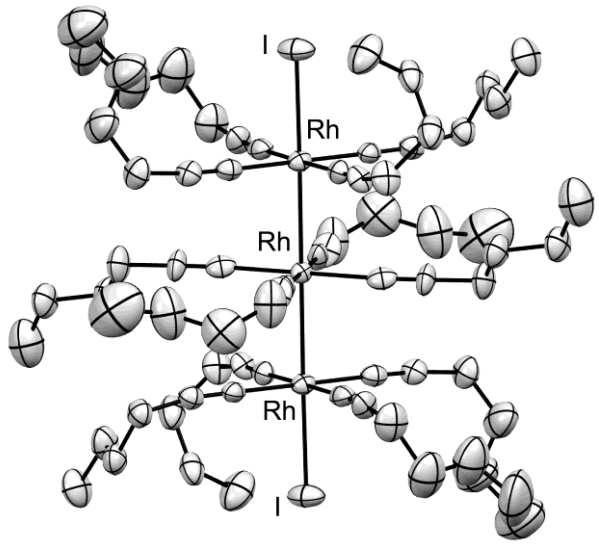

Figure S13. Molecular structure of the cation in [**3-I$_2$**][Tf_2N]$_3$. Hydrogen atoms have been omitted for clarity.

Table S1. Crystallographic parameters.

	[**1**-I_2][Tf_2N]	[**2**-I_2][Tf_2N]$_2$
Empirical formula	$C_{11}H_{18}F_3IN_{2.5}O_2Rh_{0.5}S$	$C_{44}H_{72}F_{12}I_2N_{10}O_8Rh_2S_4$
Formula weight	484.69	1684.97
Crystal system	Monoclinic	Monoclinic
Space group	$P2_1$	$P2_1/n$
a (Å)	8.790(2)	16.372(3)
b (Å)	23.162(6)	21.635(3)
c (Å)	9.029(2)	19.736(3)
α (°)	90	90
β (°)	97.105(3)	100.567(2)
γ (°)	90	90
V (Å^3)	1824.1(7)	6872.1(19)
Z	4	4
$d_{calcd.}$ (mg m^{-3})	1.765	1.629
T (K)	100	100
μ (mm^{-1})	2.338	1.583
Reflections collected	9913	38965
Independent reflections	5802	15021
R_{int}	0.0167	0.0305
F(000)	944	3352
R_1[a)], wR_2[b)] ($I > 2\sigma$(I))	0.0263, 0.0609	0.0375, 0.0935
R_1[a)], wR_2[b)] (all data)	0.0284, 0.0627	0.0512, 0.1015
Goodness-of-fit on F^2	1.128	1.035
Completeness to θ (%)	99.8	99.1
Parameters	436	747
Largest diff. peak and hole	1.308 and –0.854	1.751 and –1.167
Flack parameter	0.437(11)	

a) $R_1 = \Sigma \, ||F_o| - |F_c|| \, / \, \Sigma \, |F_o|$, b) $wR_2 = [\Sigma \, w(F_o^2 - F_c^2)^2 \, / \, \Sigma \, w(F_o^2)^2]^{1/2}$.